
Article:
Adams, PG orcid.org/0000-0002-3940-8770, Collins, AM, Sahin, T et al. (7 more authors) (2015) Diblock Copolymer Micelles and Supported Films with Noncovalently Incorporated Chromophores: A Modular Platform for Efficient Energy Transfer. Nano Letters, 15 (4). pp. 2422-2428. ISSN 1530-6984

https://doi.org/10.1021/nl504814x

Supporting Information

Diblock copolymer micelles and supported films with non-covalently incorporated chromophores: a modular platform for efficient energy transfer

Peter G. Adams,[†,1,2] *Aaron M. Collins,*[†,1] *Tuba Sahin,*[‡] *Vijaya Subramanian,*[§] *Volker S. Urban,*[⊥] *Pothiappan Vairaprakash,*[‡] *Yongming Tian,*[†] *Deborah G. Evans,*[§] *Andrew P. Shreve,*[§,*] *Gabriel A. Montaño*[†,*]

[†]Center for Integrated Nanotechnologies, Los Alamos National Laboratories, Los Alamos, NM, 87545; [‡]Department of Chemistry, North Carolina State University, Raleigh, NC, 27695; [§]Center for Biomedical Engineering, University of New Mexico, Albuquerque, NM, 87131; [‡]Department of Chemistry, New Mexico Institute of Mining and Technology, Socorro, NM 87801;[⊥]Biology and Soft Matter Division, Oak Ridge National Laboratory, Oak Ridge, Tennessee 37831.

[1] These authors contributed equally to this work

[2] Current address: School of Physics and Astronomy, University of Leeds, Leeds LS2 9JT, United Kingdom

* To whom correspondence should be addressed: gbmon@lanl.gov, shreve@unm.edu

Materials and Methods

LH nanocomposites assembly

Hydroxyl-terminated poly(ethylene oxide)-block-poly(butadiene) (PEO-b-PBD) with block weights of 1.3 and 1.2 kDa and a polydispersity index of 1.1 was purchased from Polymer Source Inc. (Quebec, Canada). BODIPY-HPC(2-(4,4-Difluoro-5,7-Dimethyl-4-Bora-3a,4a-Diaza-s-Indacene-3-Pentanoyl)-1-Hexadecanoyl-sn-Glycero-3-Phosphocholine) was purchased from Life Technologies (NY, USA). The synthetic bacteriochlorin, BC-1, was synthesized as described previously.[1]

PEO-b-PBD Polymer micelles were formed via water infusion, as follows: PEO-b-PBD, BODIPY-HPC and BC-1 were dissolved in 0.5 mL of tetrahydrofuran (THF) to give a polymer concentration of 5 mM and chromophore concentrations of (0-2.2 mol % with respect to the polymer). The concentrations of BODIPY-HPC were determined using a manufacturer supplied extinction coefficient of 83,000 $cm^{-1} M^{-1}$. The concentration of BC-1 was determined using a gravimetrically determined extinction coefficient of 40,000 $cm^{-1} M^{-1}$. Distilled water was added by a syringe pump at 2 mL/hr while the solution was stirred to give a final 1:5 ratio of THF:water. After infusion, each sample was subjected to rotary evaporation at 40 °C to remove the remaining THF. Samples were extruded five times though a 0.2 μm polypropylene membrane filter and then immediately used for subsequent spectroscopy and microscopy investigations.

Light scattering analysis

Dynamic light scattering (DLS) and static light scattering (SLS) studies were performed on a Zetasizer Nano (Malvern Instruments Ltd, Malvern, UK) using a 633 nm He-Ne laser and a detection angle of 173°.

Spectroscopy

Absorbance spectra were acquired on a Cary 6000i spectrophotometer (Agilent Technologies, CA, USA) with a 110mm- integrating sphere attachment. Steady-state and time resolved fluorescence data were acquired on a Photon Technology International (NJ, USA) fluorometer. Excitation was provided by a Xe-arc lamp for steady-state measurements and a 460 nm pulsed LED for time resolved studies. All spectroscopy data was plotted and analyzed in OriginPro software, as described in each section. Excitation and emission wavelengths are given in the figure legends.

Supported polymer bilayer/ monolayer formation

Polymer bilayers and polymer monolayers were formed by PEO-b-PBD deposition onto hydrophilic or hydrophobic substrates, respectively, as described previously.[2] Hydrophilic substrates were glass coverslips cleaned by piranha solution (3:1 H_2SO_4/30% H_2O_2, caution, highly exothermic!). Hydrophobic substrates were formed by vapor phase deposition of octyldimethylmethoxysilane onto hydrophilic glass coverslips in a vacuum oven (~120°C, 90 min). Patterned substrates were generated by microcontact printing onto hydrophilic glass coverslips, following established methods,[3] briefly described below. Polydimethylsiloxane stamp pads with a square lattice relief pattern were formed by polymerization of dimethylsiloxane on a silicon master pattern. Stamps were inked with 0.4% (w/v) octadecyltrichlorosilane (Gelest, Morrisville, PA) in toluene and used to print onto hydrophilic glass. Hydrophobic ultrathin

'imaging spacers' (Electron Microscopy Sciences, Hatfield, PA) were attached to substrates to create small wells to confine a buffer droplet creating an 'open' sample set-up to allow top-down access for exchange of liquids and atomic force microscopy. Supported polymer bilayers (and monolayers) were formed by deposition of 1 mg/mL PEO-b-PBD /chromophore micelles onto the substrate for 20 min then washed with distilled water, to remove any unbound micelles.

Fluorescence Microscopy

Fluorescence microscopy was performed on a FV-1000 inverted optical microscope (Olympus, Tokyo, Japan) equipped with multi-channel photomultiplier detectors, operated in 'photon-counting mode', acquiring 512 x 512 pixel images. A 40 x air objective (NA = 0.95) was used. Images of BODIPY fluorescence were acquired by exciting with a multi-line Ar laser (488 nm) and collecting emission using appropriate high performance band-pass filters (505-525 nm). Fluorescence recovery after photobleaching (FRAP) experiments were performed using manufacturer's provided software. For preferential bleaching of BODIPY the multi-line Ar laser (488 nm) was used; for preferential bleaching of BC-1 a HeNe laser (543 nm) was used. Image analysis was performed using ImageJ,[4] as described in Section 6.

Atomic force microscopy

Atomic force microscopy (AFM) was performed on the nanocomposite thin film samples in order to interrogate their continuity and roughness. AFM used an MFP-3D-SA system, equipped with a closed loop XY scanner and all-digital ARC2 Controller (Asylum Research, Santa Barbara, CA). All imaging was performed under fluid using Bruker SNL probes, sharpened Si tip on a triangular SiN cantilever (k ~ 0.12 N/m). High quality topographs were generally acquired at 512 x 512 pixels and 1 Hz scan speed. Images were processed using the manufacturer's provided Igor Pro-based software.

Theoretical model of polymer/ chromophore system

Energy transfer processes were modeled by assuming a random distribution of acceptor molecules surrounding each independent donor. For micelle systems, the acceptors were taken to be confined to a spherical surface for a sphere of radius 5.5 nm (corresponding to an polymer aggregate number of ≈300), where both of these values are consistent with experimental estimates and also are found to provide an excellent match to experimental data. For the small micelle systems, the number of acceptor molecules per micelle was taken to follow a Poisson distribution with mean value, divided by the polymer aggregation number, corresponding to the mole percent of acceptors. Details of the theoretical modeling of the polymer/chromophore system are provided in Section 5, below.

Small Angle Neutron Scattering

Small-angle neutron scattering (SANS) data were measured using the CG-3 Bio-SANS instrument[5, 6] at the High-Flux Isotope Reactor of Oak Ridge National Laboratory. Neutron wavelength was 6Å with a wavelength spread 15% FWHM. Two instrument configurations were employed with 2.53 m and 15.33 m sample-to-detector distance and with 17.43 m collimation length from source aperture to sample aperture in both configurations. The solution samples were contained in circular quartz cuvettes with 2mm path length and measured at 20° C. Neutron

scattering and transmission data were collected on a position-sensitive 1x1 m^2 ^{3}He detector tube array.[7] Raw SANS data sets were processed with in-house analysis routines.[8]

Section 1: Polymer micelle size and morphology

Analysis of light scattering for polymer micelle size and aggregation number

The micellar weight-average molecular weight (M_w) was established from the linear portion of the concentration dependence of the reduced SLS intensity according to the following equation[9]:

$$\frac{KC}{R_\theta} = \left(\frac{1}{M_w} + 2A_2C\right) \quad \text{(S1)}$$

Where K is an optical constant that depends on the differential refractive index, dn/dC, C is the sample concentration, R_θ is the Rayleigh ratio of scattered to incident light intensity, M_w is the weight-average molecular weight, and A_2 is the second virial coefficient. dn/dC, used in the calculation of the M_w was 0.125 ml/g for PEO-b-PDB.[10] Further details of the static light method and theory can be found elsewhere.[11] By this method, M_w for PEO-b-PBD micelles was determined to be 6.2 x 10^5 Da (Figure S1C). Given that the individual chain PEO-b-PBD molecular weight is 2500 g/mol, the aggregation number is calculated to be ~248.

DLS was performed on fresh polymer micelle samples to determine their hydrodynamic diameter. Examination of the DLS scattering data suggests there is a bimodal distribution of aggregates in the sample (Figure S1A) with hydrodynamic diameters of approximately 20 nm and 200 nm. Conversion of the scattering intensity to a volume distribution using the instrument software reveals that the overwhelming majority (99.99%) of the sample volume is in the form of smaller micelles (Figure S1B). Even though there are a low number of larger particles, they must be considered in the determination of the aggregation number as they are significantly more massive than the micelles and will contribute to M_w as determined from SLS. If it is assumed that the larger aggregates are an association of micelles with an identical density, the molecular weight of the micelles (M_1) and micelles clusters (M_2) can be determined from M_w following:

$$M_W = W_1M_1 + W_2M_2 = M_1(W_1 + nW_2) \quad \text{(S2)}$$

where W_1 and W_2 are the fractional volume distribution of the micelles and micelle clusters (W_1 = 0.9999; W_2 = 0.0001) , respectively, and n is the ratio of volumes of the larger cluster to micelle (n = 1000), assuming both are spherical. This yields weight-average molecular weights for the micelles and micelle clusters of 5.6 x 10^5 Da and 6.0 x 10^8 Da, respectively. Finally, dividing M_1 or M_2 by the individual polymer molecular weight gives aggregation numbers of approximately 225 and 2.4x10^5 for the micelles and aggregated clusters, respectively.

From the aggregation number, the core radius can be estimated by assuming the core is spherical and comprised of only polybutadiene following,[12]

$$r_c = \left(\frac{3M_nW_{PBD}N_{agg}}{4\pi\rho_{PBD}}\right)^{1/3} \quad \text{(S3)}$$

where M_n is the copolymer molecular weight, W_{PBD} is the weight fraction of polybutadiene, N_{agg} is the aggregation number and ρ_{PBD} is the density of pure polybutadiene (0.87 g cm^{-3}). This analysis gives a core radius of 5.0 nm with agrees favorably with the core radius as determined from neutron scattering.

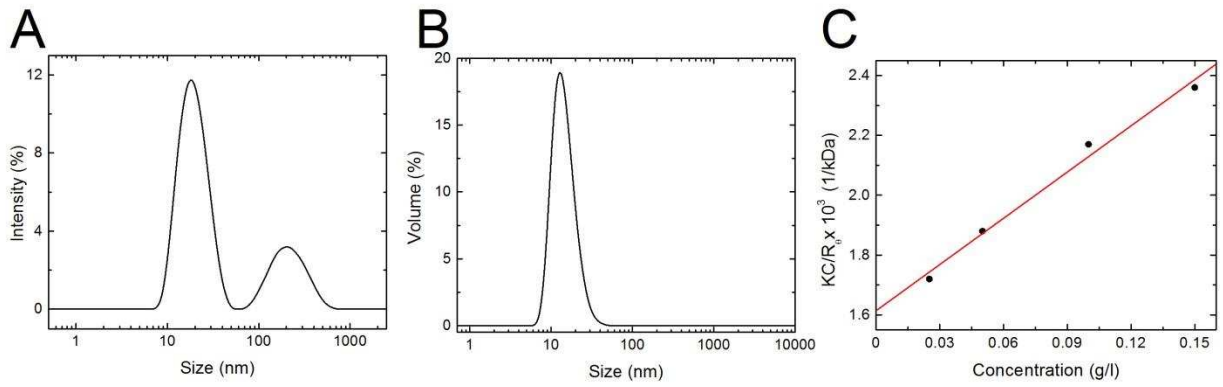

Figure S1. (A) DLS Intensity particle size distribution of micelle size. The hydrodynamic diameters were determined to be ~20 and 200 nm, respectively. (B) Volume distribution of the same data in presented in (A). (C) Debye plot of the reduced scattering intensity (derived from SLS) versus concentration for PEO-b-PBD. The red line represents a linear fit to the data.

Small Angle Neutron Scattering

Samples were prepared for SANS experiments using the protocol as described above to generate PEO-b-PBD polymer micelles at a range of polymer concentrations, except that no chromophores were included and D_2O was used rather than H_2O. A dilution series was studied with polymer concentrations of 5g/L, 3g/L, 1g/L, and 0.5g/L, respectively. The background-corrected SANS data of the concentration series is shown in Figure 1E of the main article. The Q-dependence of the scattering intensity is similar for all four samples over most of the observed Q-range with small deviations in the initial slope at $Q < 0.01$. This finding is further illustrated in Figure S2 by plotting the intensities divided by the polymer concentration. As expected for correct accounting of sample concentration the curves overlay perfectly within the statistical measurement uncertainty, except for the systematic deviation at very small Q.

The lin-log plot in (Figure S2A) shows a bell-shaped drop of intensity with a secondary maximum. Such signatures are typical for scattering form factors of well-defined particle shapes with relatively narrow polydispersity. Conversely, the upturn at $Q < 0.01$ $Å^{-1}$ appears in the lin-log representation as a signal that is additive to an underlying scattering form factor. Three scenarios can generally cause such a low-Q upturn: a) (attractive) inter-particle interaction,[13] b) larger associates of the primary particle—this includes the case of anisometric particles, such as rods, which can be thought of as linear assemblies of smaller units; in that case the cross section

produces a form factor at high Q, while the linear dimension produces a power-law upturn[8] at lower Q—and c) presence of larger species in addition to the primary scattering object that produces the form factor scattering. Importantly, in this experiment the "up-turn" scattering intensity decreases with increasing concentration, which is contrary to what one would expect for scenario a), which therefore does not seem to be a likely explanation. Scenario b) generally leads to power-law scattering at low Q. The apparently quite linear section at Q < 0.01 Å^{-1} in the log-log representation in Figure S2B would indeed suggest a power-law, however, a fit to the data in this region leads to power-law exponents with magnitude significantly smaller than 1, which does not correspond to any physical models. Therefore, the likely scenario is c) the presence of a minority component of larger scattering objects in addition to the majority component of smaller scattering objects in agreement with observations from the DLS results above.

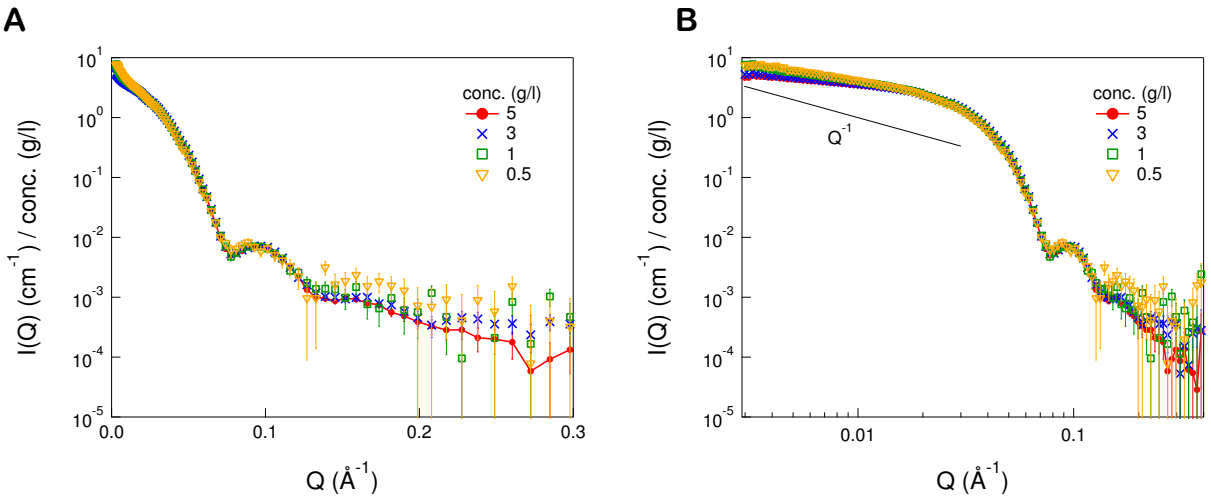

Figure S2. Neutron scattering intensity I(Q) plotted against the magnitude of the scattering vector Q in a lin-log (A) and log-log (B) representation. In this representation the neutron scattering data was divided by the respective concentration to more clearly observe potential concentration-dependent differences in micelle size or structure. The data sets overlay within statistical errors (error bars shown), except for a trend of small discrepancies at low scattering vectors Q < 0.01 Å^{-1}.

The data with Q > 0.01 Å^{-1} was analyzed further by attempting different form factor fits,[14] with a spherical core-shell model with modest polydispersity of the core radius fitting the scattering data very well (Figure 1E of the main article). Moreover, the location of the shoulder and peak and the intensity of the peak relative to the intensity at the lower Q shoulder provide three strong constraints that allow a fairly accurate determination of the core radius (57 Å), shell thickness (33 Å) and scattering length density contrast ratio of the core vs. shell (10); the latter result implies significant D_2O concentration in the shell.

Section 2: Polymer micelle chromophore content

Comparison of absorbance spectra of the BC-1 and BODIPY-HPC chromophores in organic solvent and within PEO-b-PBD micelles

The spectra for both chromophores are broadly similar when comparing the starting material, fully solvated pigments in tetrahydrofuran, to the chromophores after their incorporation into the hydrophobic core of polymer micelles, in water (Figure S3). For BODIPY-HPC, the peak maximum is at ~508 nm for both THF and in polymer micelles. For BC-1, the Q_x and Q_y red shift and broaden slightly from THF to polymer micelles (Q_x max: shift from ~513 to 518 nm; Q_y max: shift from ~728 to 733 nm).The shift in the maximum of BC-1 is not unexpected, and reflects the change in local environment of BC-1 molecules and interactions with the different solvent (organic solvent to PEO/PBD).

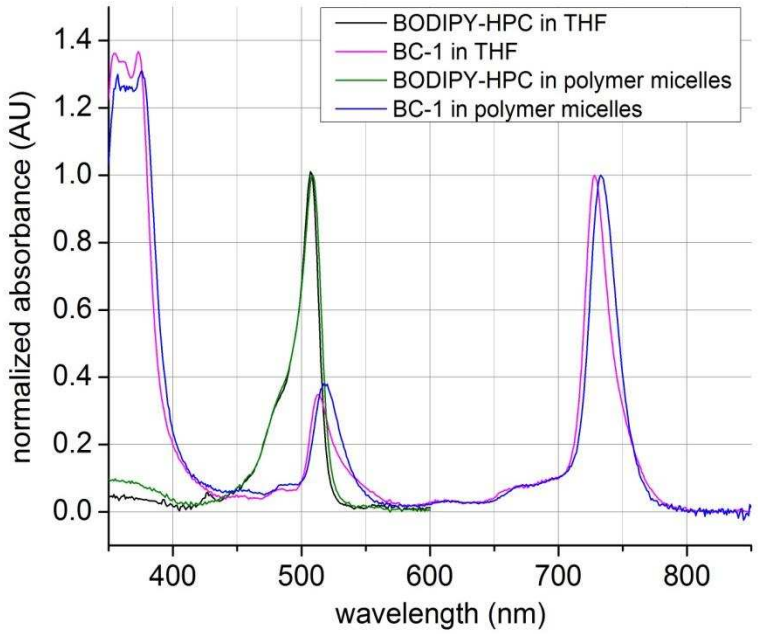

Figure S3. Absorbance spectra for BC-1 and BODIPY-HPC in THF and incorporated into polymer micelles. The data have been normalized to an absorbance of 1.0 for the peak of interest.

Section 3: Analysis of spectroscopy data

Analysis of absorbance spectra to calculate the relative chromophore concentrations in polymer micelles

The average chromophore concentration in each micelle preparation can be determined from each samples absorbance and is necessary for accurate determination of energy transfer. The long wavelength band of the BC-1 chromophore does not overlap with BODIPY and therefore its concentration in the micelles can be determined from the integrated area (650-800 nm) of this absorbance band (see Figure S4A) and comparison against a standard curve.

For each sample described in the main article, the integrated areas were measured in this manner and the BC-1 concentration was estimated by comparison to a standard curve of BC-1 integrated areas versus known concentration, generated from PEO-b-PBD samples containing a range of BC-1 but zero BODIPY-HPC. Figure S4B shows how the raw spectrum can be analyzed to estimate the BODIPY concentration. The BODIPY band overlaps with the BC-1 Q_x band, so their respective contributions must be determined. To this end, the spectrum from the sample containing both chromophores (red) is normalized to a spectrum for a standard BC-1-only sample (blue) using the long wavelength peak where there is no overlap of features and the spectra are subtracted to generate a new spectrum (brown) that contains only the contribution from the BODIPY band. These new spectra are checked against polymer/BODIPY-only samples to confirm that the residuals are low and they are then integrated over wavelengths between 425-550 nm. For each sample described in the main article, integrated areas measured in this manner were compared to a standard curve of BODIPY-HPC integrated areas versus known concentration, where the latter was generated from PEO-b-PBD samples containing a range of BODIPY-HPC but zero BC-1. Form this procedure the BODIPY-HPC concentration was determined for each sample.

Analysis of emission spectra to calculate ETE

Figure S4C shows an example of a steady-state fluorescence emission spectrum of (i) a sample containing PEO-b-PBD with 0.54% BODIPY-HPC and 2.13% BC-1 (blue), compared to (ii) a sample containing PEO-b-PBD with 0.50% BODIPY-HPC and no BC-1 (green). These emission spectra excitation were acquired as described in the Methods, with excitation at 469 nm (4 nm bandwidth) and collection between 480-700 nm (1 nm bandwidth).

For each sample containing both donor and acceptor chromophores, the energy transfer efficiency (ETE) was calculated based on the relationship:

$$ETE = 1 - \frac{F_{DA}}{F_D} \quad \text{(S4)}$$

where F_{DA} was the calculated integrated area between 480-650 nm of the donor and acceptor sample and F_D was the "donor-only" integrated emission extrapolated from a standard curve of integrated areas of BODIPY emission against known concentration, generated by measuring emission spectra for a series of PEO-b-PBD samples containing a range of BODIPY-HPC (without any BC-1). In this way, the F_D represents the integrated emission of a sample with an identical concentration of donor. ETE was then calculated following the formula above.

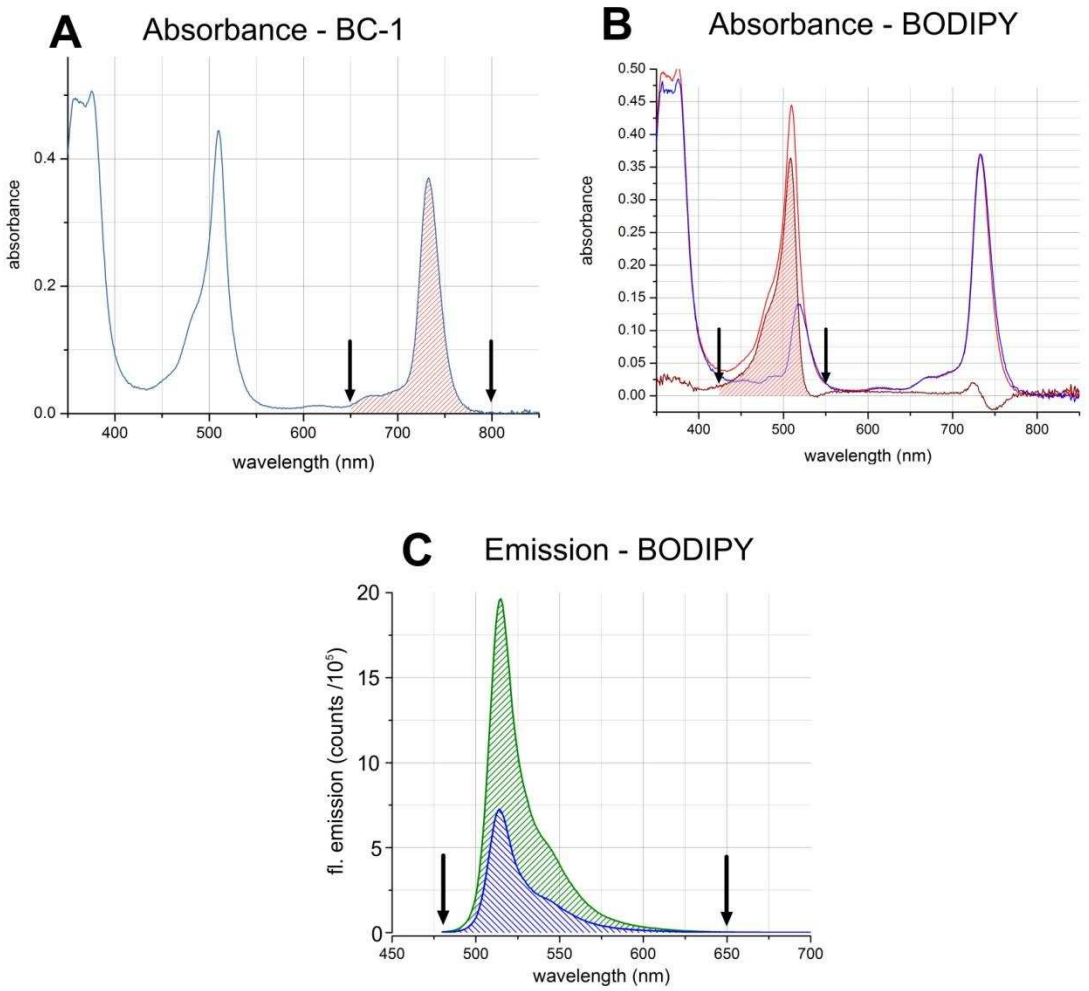

Figure S4. Analysis of absorbance and emission spectra. Panels (A)-(B), show an example of an absorbance spectrum for a polymer nanocomposite sample of PEO-b-PBD containing 1% BODIPY-HPC and 1% BC-1. Panel (A) highlights the area the integrated area between 650-800 nm that represents the BC-1 Q_y band. In (B), the contribution from BODIPY-HPC (brown) is derived by subtracting a Q_y-normalized spectrum (blue) from sample containing both chromophores (red). (C) BODIPY emission spectra (excitation =469 nm) for micelle samples containing PEO-b-PBD with 0.54% BODIPY-HPC and 2.13% BC-1 (blue) and 0.50% BODIPY-HPC and no BC-1 (green). For analysis of energy transfer, the spectra are integrated between 480-650 nm.

Section 4: Further fluorescence spectroscopy data

Further data of steady state and time-resolved fluorescence spectroscopy

Figures S5 and S6 provide the full extent of the fluorescence data that was analyzed to provide ETE shown in Table 1 and 2 in the main article.

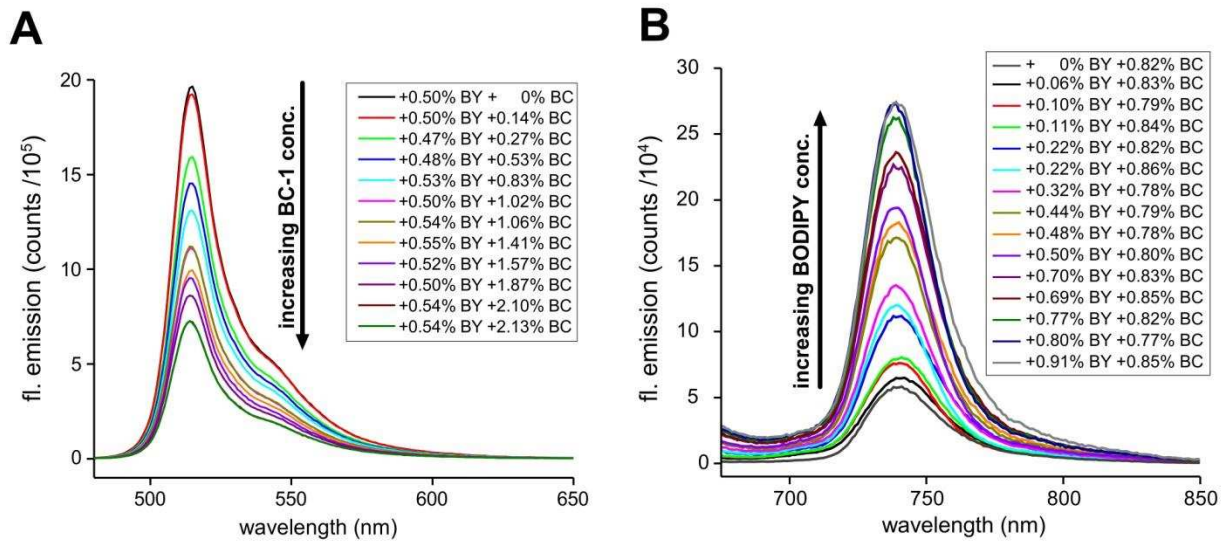

Figure S5. Full datasets for steady-state fluorescence emission. This figure is equivalent to that from the main article Figure 2, panels (A) and (B), except that we are able to display more data with the additional space allowed in the Supporting Information. (A) Set 1, emission spectra of the BODIPY peak (excitation at 469 nm, 4 nm bandwidth, collection between 480-650 nm, 1 nm bandwidth). (B) Set 2, emission spectra of the BC-1 peak (excitation at 469 nm, 4 nm bandwidth, collection between 650-850 nm, 4 nm bandwidth). Legend shows BODIPY-HPC concentration ("% BY") and BC-1 concentration ("%BC") in each LH nanocomposite sample.

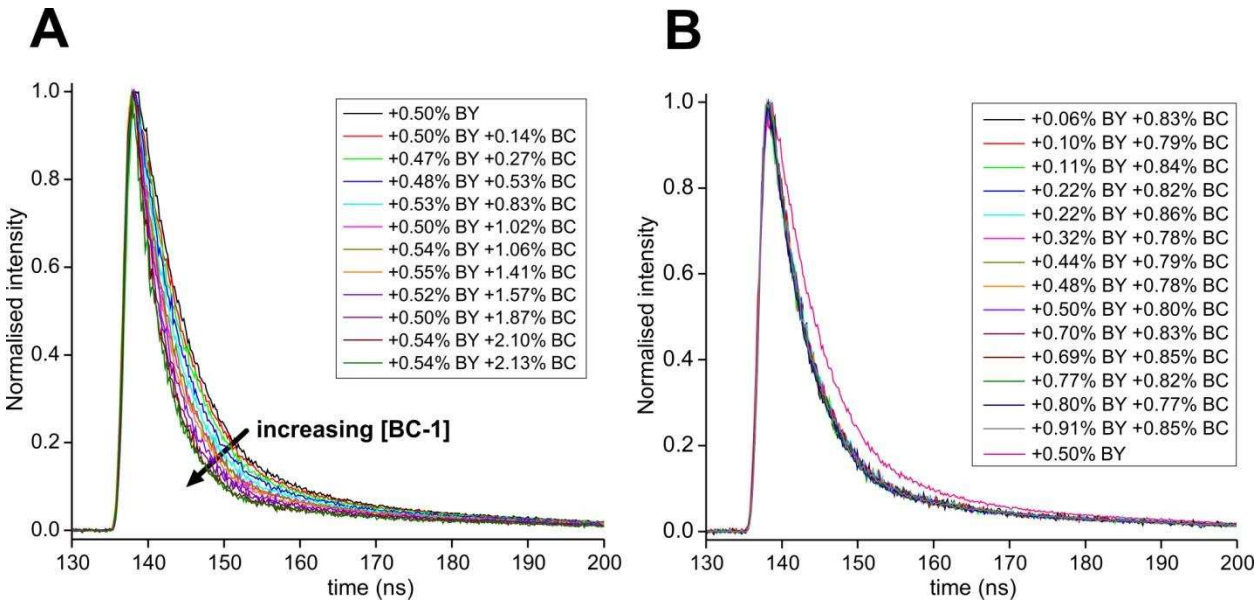

Figure S6. Full datasets for time-resolved fluorescence decay curves. Decay curves of BODIPY

fluorescence with excitation provided by a 465 nm LED and emission collected at 514 nm (12 nm bandwidth). Curves are normalized to a peak intensity of 1.0. Panel (a) is similar to Figure 2c in the main article, decay curves for Set1 (range of BC-1 and constant BODIPY-HPC) samples, except that we are able to display more data with the additional space allowed in the Supporting Information. Panel (B) shows the data for Set 2 (range of BODIPY-HPC and constant BC-1), which were not displayed in the main article due to space limitations.

sample #	[BODIPY-HPC] (%)	[BC-1] (%)	ETE steady-state	ETE lifetime
1	***0.50***	***0***	***-***	***-***
2	0.51	0.14	0.03	-
3	0.47	0.27	0.14	-
4	***0.48***	***0.53***	***0.22***	***0.23***
5	0.53	0.83	0.36	-
6	***0.50***	***1.02***	***0.42***	***0.40***
7	0.54	1.06	0.47	-
8	0.55	1.41	0.53	-
9	***0.52***	***1.57***	***0.53***	***0.55***
10	0.50	1.87	0.56	-
11	0.54	2.10	0.65	-
12	***0.54***	***2.13***	***0.66***	***0.65***

Table S1. Analysis of energy transfer efficiency from Set 1 (comparable BODIPY).
'ETE steady-state' refers to the energy transfer efficiency calculated from the analysis of fluorescence emission experimental data. 'ETE lifetime-based' refers to the efficiency predicted from the theoretical model of the system, which predicted fluorescence decay curves (main article Figure 2D). Samples shown in ***bold*** are the samples for which fluorescence emission spectra (main article Figure 2A) and experimental and theoretical fluorescence decay curves (main article Figure 2D) are shown. All samples are used as data points for the plot of ETE vs. [BC-1] in main article Figure 3.

sample #	[BODIPY-HPC] (%)	[BC-1] (%)	ETE steady-state
13	***0***	***0.82***	**-**
14	0.06	0.83	0.38
15	0.10	0.79	0.44
16	***0.11***	***0.84***	***0.47***
17	***0.22***	***0.82***	***0.42***
18	0.22	0.86	0.41
19	0.32	0.78	0.39
20	***0.44***	***0.79***	***0.39***
21	0.48	0.78	0.35
22	0.50	0.80	0.44
23	***0.70***	***0.83***	***0.39***
24	0.69	0.85	0.42
25	0.77	0.82	0.40
26	0.80	0.77	0.41
27	***0.91***	***0.85***	***0.42***

Table S2. Analysis of energy transfer efficiency from Set 2 (constant BC-1)
'ETE steady-state' refers to the energy transfer efficiency calculated from the analysis of fluorescence emission experimental data. Samples shown in ***bold*** are the samples for which fluorescence emission spectra are shown in main article Figure 2B. These data are shown in the extended plot of ETE vs. [BC-1] in Supplementary Figure S7, below.

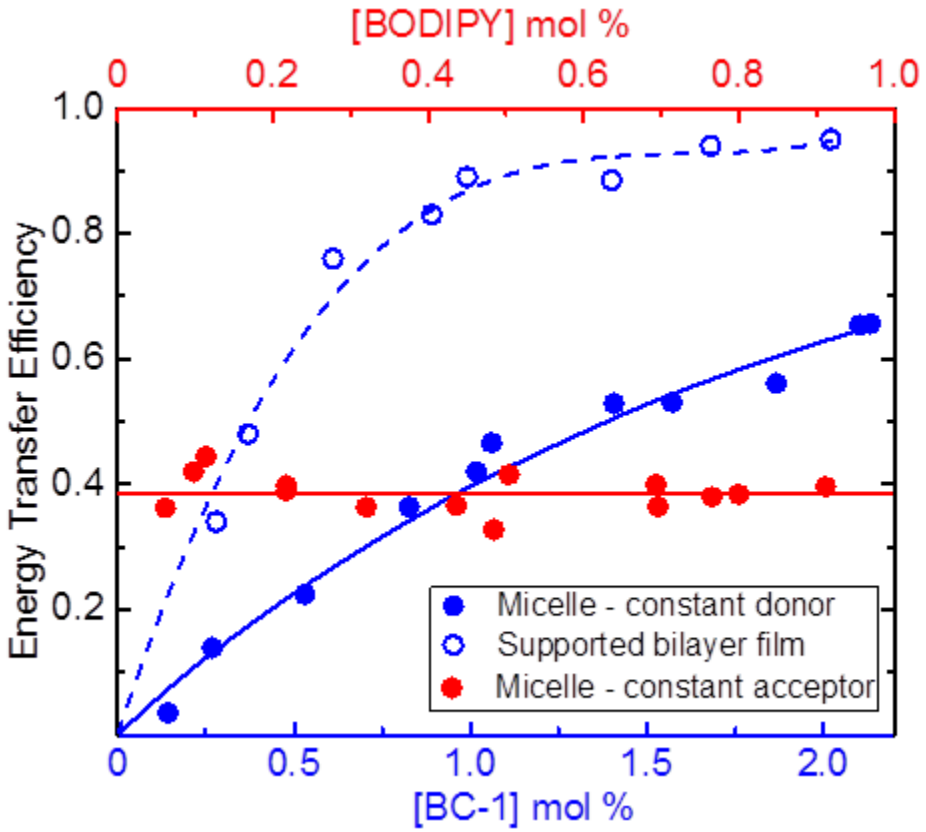

Figure S7. Full datasets plotted for ETE vs. concentration of each chromophore. ETE for polymer micelles from Set 1 plotted against BC-1 concentration, (constant BODIPY-HPC ~0.5%) (solid blue circles); ETE for polymer micelles from Set 2 plotted against BODIPY-HPC concentration, (constant BC-1 ~0.8%) (solid red circles); ETE for supported polymer bilayer films plotted against BC-1 concentration, (similar BODIPY-HPC ~0.6%) (open blue circles). See Tables S1, S2 and S3. As a guide, fits to the data are shown using a straight line (red) or polynomials (dashed and solid, blue).

Section 5: Theoretical model of the polymer/ chromophore system

The basic theoretical model follows an approach presented by Wolber and Hudson,[15] building upon initial work by Förster, where the rate constant for Förster resonance energy transfer between donor and acceptor chromophores depends on the inter-chromophore distance and is given by[16]

$$k = 1/\tau_0 \, (R_0/R)^6 \tag{S5}$$

Here R is the inter-chromophore distance, R_0 the Forster radius, at which the energy transfer efficiency is 0.5, and τ_0 is the excited state lifetime of the donor in the absence of the acceptor. For multiple (N) acceptors, the rate of donor excitation decay, in terms of the survival probability of donor excitation, p(t), and in the limit of low concentration of donors and acceptors is given by

$$-\frac{dp(t)}{dt} = \tau_0{}^{-1}\left(1 + \sum_{i=1}^{N} (R_0/R_i)^6\right)p(t) \tag{S6}$$

where R_i is the distance between the donor and the i^{th} acceptor.

Solving for $p(t)$ yields

$$p(t) = e^{-t/\tau_0} \prod_{i=1}^{N} e^{-t/\tau_0 (R_0/R_i)^6} \tag{S7}$$

In a system with a uniform random distribution of acceptors around the donor, an ensemble average of the excitation energy decay over a distance distribution function, W(R), which gives the probability of finding an acceptor at a given distance, R, from the donor, will have to be considered.[15, 16] For micelles, we choose to model the amphiphilic chromophores as being distributed uniformly on the surface of a sphere defined by the hydrophobic core of the micelle, while for planar films, the chromophores are taken to be uniformly distributed on a two-dimensional disk. The distance distribution functions for the case of donor and acceptors distributed on the surface of a sphere and a disk are $R/2R_d{}^2$ and $2R/R_d{}^2$ respectively.[17] The ensemble average is then given by,

$$< p(t) >_n = e^{-t/\tau_0} \prod_{i=1}^{N} \int_{R_e}^{R_d} e^{-t/\tau_0 (R_0/R_i)^6} W(R) dR \tag{S8}$$

where R_d is the radius of the disk or sphere and R_e is the distance of closest approach of donor and acceptor.

In addition to the ensemble average over the distribution of distances between donor and acceptor, another factor to consider is the distribution in the number of acceptors in the micelles. The loading of acceptors within the micelles is expected to follow a Poisson distribution at the low concentrations studied.[18] Thus, in calculations of donor excitation decay, the number of acceptors in a micelle was drawn from a Poisson distribution and the average value of the survival probability at each time point was determined.

The efficiency of excitation energy transfer is defined in terms of the quantum yield of excitation transfer in the presence and absence of the acceptors as follows:

$$E = 1 - q_{DA}/q_D \quad \text{(S9)}$$

where the subscripts DA and D refer to the cases where both donor and acceptor are present or just donor is present, respectively. For each case, q is calculated as

$$q = \int_0^\infty < p(t) > dt \quad \text{(S10)}$$

All calculations were carried out using Mathematica 9. The value of R_0 was determined 4.2 nm from the overlap of the donor chromophore emission and absorbance of the acceptor chromophore according to,

$$R_0 = \left(\frac{9000(\ln 10)\kappa^2 q_D}{128\pi^5 N_A n^4} \int_0^\infty F_D(\lambda)\varepsilon_A(\lambda)\lambda^4 d\lambda\right)^{1/6} \quad \text{(S11)}$$

where κ^2 is an orientation factor, N_A is Avogadro's number, n is the refractive index of the medium (1.5 for polybutadiene), $F_D(\lambda)$ is the fluorescence intensity of the donor at a given wavelength and $\varepsilon_A(\lambda)$ is the extinction of the acceptor at a given wavelength.[19] R_e in equation (S8) was typically set to 0.1 nm (though the results were verified to be independent of the specific choice of R_e for relatively large variations around this value for the concentration ranges studied here). The concentrations used were based on the experimental mole percentages and the average number of acceptors, N, was determined using a micelle aggregation number of 300 and corresponding radius of the hydrophobic core, R_d, of 5.5 nm. These values are intermediary from estimates of the aggregation number and core radius from SLS and SANS analysis. Other values of the aggregation number were tested, ranging from 100 to 700 in increments of 100, but 300 was found to provide the best match to experimental results and is also in close agreement with experimental estimates. The average in Eqn. S8 was carried out by sampling 3000 times from a Poisson distribution with mean value of acceptors determined from the concentration. The integral in Eqn. S9 was evaluated numerically with the upper integration limit set at 7 in dimensionless units of t/τ_0. For comparison with experimental data, τ_0 was set to 6.5 nsec, as determined by fitting experimental data BODIPY-HPC containing micelles with no acceptor present. In all cases, comparison with experiments was also facilitated by convolving calculated decay curves with the experimentally determined instrument response function for the time-resolved measurement.

Section 6: Further data on supported films

Analysis of fluorescence counts

For each sample, the mean fluorescence intensity counts were measured from a 40 x 40 μm field using ImageJ and averaged for 5-10 independent regions. For comparability, samples of PEO-b-PBD with both chromophores were analyzed in parallel, on the same coverslip, with a control sample of PEO-b-PBD with only donor chromophores. ETE was calculated using Eqn. 1, using the values for averaged fluorescence intensity for the donor+acceptor sample (F_{DA}) vs the donor-only sample (F_D).

Further data on polymer bilayers

Data from analysis of polymer bilayers vs polymer micelles, displayed in a numerical form, corresponding to the data displayed in the main article Figure 3.

[BC-1] (%)	[BODIPY-HPC] (%)	ETE (surface)	ETE (solution)
0.00	0.56	-	-
0.00	0.54	-	-
0.00	0.62	-	-
0.28	0.57	0.34	0.19
0.37	0.57	0.48	0.21
0.61	0.59	0.77	0.27
0.89	0.59	0.84	0.40
0.99	0.66	0.90	0.51
1.41	0.60	0.89	0.54
1.68	0.57	0.94	0.71
2.02	0.68	0.95	0.67

Table S3. Fluorescence intensity analysis in polymer bilayers. Samples were prepared as micelle assemblies for determination of chromophore concentrations and solution-based ETE efficiency and then deposited onto a glass substrate (see material and methods).

Comparison of lipid bilayers with polymer bilayers

Lipids used were the common fluid-phase phospholipid 1,2-dioleoyl-sn-glycero-3-phosphocholine (DOPC). Lipid vesicle/ chromophore nanocomposite samples were prepared using the same protocol as for polymer/ chromophore samples, starting with 5 mM DOPC in THF. This preparation was characterized by DLS and resulted in liposomes of average diameter of 260 nm. Two different samples were prepared at the chromophore concentrations shown below (note, the chromophore concentrations stated are mol% relative to the DOPC concentration). Samples were analyzed in the same manner as for polymer samples, to calculate ETE in the aqueous-based lipid vesicles and for supported lipid bilayers formed by deposition of the vesicles onto hydrophilic glass coverslips:

[BC-1] (%)	[BODIPY-HPC] (%)	ETE (surface)	ETE (solution)
0.00	0.39		-
0.98	0.47	0.69, 0.73*	0.71

* technical replicates

Table S4. Fluorescence intensity analysis in lipid bilayers.

As shown in the table, there is no significant difference between the energy transfer efficiency for lipid vesicles compared to the bilayers. This suggested that the distribution of chromophores did not change significantly due to film formation, in contrast to the significantly increased ETE observed for PEO-b-PBD films.

References

(1) Aravindu, K.; Mass, O.; Vairaprakash, P.; Springer, J. W.; Yang, E.; Niedzwiedzki, D. M.; Kirmaier, C.; Bocian, D. F.; Holten, D.; Lindsey, J. S. Chem. Sci. **2013,** 4, 3459-3477.

(2) Goertz, M. P.; Marks, L. E.; Montaño, G. A. **2012,** 6, 1532-1540.

(3) Whitesides, G. M.; Ostuni, E.; Takayama, S.; Jiang, X.; Ingber, D. E. Annu. Rev. Biomed. Eng. **2001,** 3, 335-373.

(4) Abràmoff, M. D.; Magalhães, P. J.; Ram, S. J. Biophotonics Int. **2004,** 11, 36-43.

(5) Heller, W. T.; Urban, V. S.; Lynn, G. W.; Weiss, K. L.; O'Neill, H. M.; Pingali, S. V.; Qian, S.; Littrell, K. C.; Melnichenko, Y. B.; Buchanan, M. V.; Selby, D. L.; Wignall, G. D.; Butler, P. D.; Myles, D. A. Appl. Crystallogr. **2014,** 47, 1238-1246.

(6) Lynn, G. W.; Heller, W.; Urban, V.; Wignall, G. D.; Weiss, K.; Myles, D. A. A. Phys. B **2006,** 385-86, 880-882.

(7) Berry, K. D.; Bailey, K. M.; Beal, J.; Diawara, Y.; Funk, L.; Hicks, J. S.; Jones, A. B.; Littrell, K. C.; Pingali, S. V.; Summers, P. R.; Urban, V. S.; Vandergriff, D. H.; Johnson, N. H.; Bradley, B. J. Nucl. Instrum. Methods Phys. Res., Sect. A **2012,** 693, 179-185.

(8) Urban, V. Small Angle Neutron Scattering. In Characterization of Materials; Kaufmann, E. N., Ed. Wiley: New York, 2012; pp 1–16.

(9) Wyatt, P. J. Anal. Chim. Acta **1993,** 272, 1-40.

(10) Fuetterer, T.; Nordskog, A.; Hellweg, T.; Findenegg, G. H.; Foerster, S.; Dewhurst, C. D. Phys. Rev. E **2004,** 70, 041408.

(11) Evans, D. F.; Wennerström, H. Structure and Properties of Micelles. In The Colloidal Domain: Where Physics, Chemistry, Biology, and Technology Meet; Wiley-VCH: New York, 1999; pp 153-210.

(12) Xu, R.; Winnik, M. A.; Hallett, F. R.; Riess, G.; Croucher, M. D. Macromolecules **1991,** 24, 87-93.

(13) Zimm, B. H. J. Chem. Phys. **1948,** 16, 1099-1116.

(14) Pedersen, J. S. Adv. Colloid Interface Sci. **1997,** 70, 171-210.

(15) Wolber, K. P.; Hudson, B. S. Biophys. J. **1979,** 28, 197-210.

(16) Förster, T. Z. Naturforsch. **1949,** 4a, 321-327.

(17) Mathai, A. M., An Introduction to Geometrical Probability: Distributional Aspects with Applications. Gordan and Breach: Newark, 1999.

(18) Finger, K. U.; Marcus, A. H.; Fayer, M. D. J. Chem. Phys. **1994,** 100, 271-286.

(19) Lakowicz, J. R. Energy Transfer. In Principles of Fluorescence Spectroscopy; Springer: Dordrecht, 2006; pp 443–475.